Visualizing Multiple Error-Sensitivity Fields for Single Camera Positioning

David H. S. Chung · Matthew L. Parry · Philip A. Legg · Iwan W. Griffiths · Robert S. Laramee · Min Chen

Abstract In many data acquisition tasks, the placement of a real camera can vary significantly in complexity from one scene to another. Optimal camera positioning should be governed not only by least error sensitivity, but in addition to real-world practicalities given by various physical, financial and other types of constraints. It would be a laborious and costly task to model all these constraints if one were to rely solely on fully automatic algorithms to make the decision. In this work, we present a study using 2D and 3D visualization methods to assist in single camera positioning based on error sensitivity of reconstruction and other physical and financial constraints. We develop a collection of visual mappings that depict the composition of multiple error sensitivity fields that occur for a given camera position. Each camera position is then mapped to a 3D visualization that enables visual assessment of the camera configuration. We find that the combined 2D and 3D visualization effectively aids the estimation of camera placement without the need for extensive manual configuration through trial and error. Importantly, it still provides the user with sufficient flexibility to make dynamic decisions based on physical and financial constraints that can not be encoded easily in an algorithm. We demonstrate the utility of our system on two real-world applications namely snooker analysis and camera surveillance.

Keywords Multi-field Visualization · Glyph-based Techniques · Uncertainty Visualization

D. H. S. Chung
Department of Computer Science, Swansea University
E-mail: D.H.S.Chung@swansea.ac.uk

M. L. Parry
Department of Computer Science, Swansea University
E-mail: M.L.Parry@swansea.ac.uk

P. A. Legg
Department of Computer Science, University of Oxford
E-mail: Phil.Legg@cs.ox.ac.uk

I. W. Griffiths
College of Engineering, Swansea University
E-mail: I.W.Griffiths@swansea.ac.uk

R. S. Laramee
Department of Computer Science, Swansea University
E-mail: R.S.Laramee@swansea.ac.uk

M. Chen
Oxford e-Research Centre, University of Oxford
E-mail: M.Chen@oerc.ox.ac.uk

1 Introduction

Multi-field visualization is concerned with the depiction of data that encodes information about multiple fields (e.g., scalar, vector and tensor fields) that are co-located in the same domain. These are usually obtained from different sampling sources or computational processes. In this work, we address the needs for visualizing error sensitivity associated in 3D scene reconstruction, which is a common modelling method in computer graphics (e.g., [31]). Error-sensitivity analysis is one approach for selecting an optimal camera position within a given scene. There are two main types of camera positioning problems. On one hand, we have the selection of virtual cameras for conveying the most information to the user. On the other, there is the task of positioning a real camera for optimizing vision-based applications. This paper focuses on the latter. In 3D reconstruction, errors in estimating camera extrinsic parameters are the most fundamental errors, which may be caused by a variety of reasons, including errors in image processing (e.g., edge detection), feature analysis (e.g., corner recognition) and geometric correlation. This leads to

Fig. 1 Constraint maps of a sample snooker room wall (Left) and a construction scene (Center) with dynamic constraints (Right). The green region highlights valid camera mounting positions with invalid positions mapped to red. The construction scene images correspond to the right wall of the camera surveillance scene in Fig. 7.The focus region must be fully in view of the camera for a position to be considered as valid.

multiple error sensitivity fields which need to be visualized together.

Statistical analyses on one or more error sensitivity fields is often used to analyze complex parameter spaces, for example, by computing an average error field, or identifying the camera with least error sensitivity based on magnitude. However, it is difficult for such statistics to convey the detailed information such as error distribution and orientation in different fields and in different parts of a field. In many real-world applications, error analysis must also be combined with other observations and practical constraints. For example, in 3D reconstruction, the best camera position is not always determined by the lowest error sensitivity. Additional knowledge such as feasibility of the camera position (i.e., windows, picture frames, scaffolding), mounting equipment cost, and impact on the environment (e.g., spectators, pedestrian and players) will heavily influence a user's decision as shown in Fig. 1. Such factors are fundamental to the planning process especially when constraints are dynamic, and when a system needs to meet the specific demands of a practical framework (e.g., portable camera systems versus a permanent setup). This is often desirable since many venues, coaching rooms, and outdoor environments are multi-purpose and require a flexible solution. Therefore, we need to investigate camera placement and their associated sensitivity in a three-dimensional search space.

Given a set of camera positions and error sensitivity fields, a typical approach for finding an optimal solution would be to use Machine Learning [1,27]. The process of machine learning involves modeling the problem (e.g., the requirements for camera placement) as formal parameters which are optimized. Due to the range of possible camera configurations in addition to the practical requirements of a user, encoding such semantic knowledge with attached weighting parameters into an algorithm is highly impractical due to costs in labor. This problem motivates us to explore a novel solution by introducing visualization as an effective planning tool for optimal placement of a camera. A visualization solution is desirable for informing the user of the error sensitivity in both a comparative and summative manner, while empowering the user to bring additional information and knowledge into the analysis.

We present a study using 2D and 3D visualization methods to assist in single camera positioning based on the error sensitivity of reconstruction. The goal of our visualization is to visually compare candidate camera positions through their associated error sensitivity, and to provide visual suggestions for estimating an optimal camera position. We find that visualization provides a faster, and cost-effective alternative over other viewpoint selection methods for real cameras and enables the user to make dynamic decisions that integrate trade-offs between reconstruction quality and feasability. In particular, the main contributions of this paper are:

– We develop a novel collection of glyph-based visualizations which depict multiple error sensitivity fields. These visual mappings can be used to evaluate prospective camera positions.
– We provide a visual summary of camera positions in a given 3D context visualization. This effectively aids the estimation of the best single camera position by enabling the user to incorporate physical, financial and other types of constraints into the decision process.
– We demonstrate the usefulness of our visualization method on two real-world applications with feedback from end-users. We note that for the application we present, financial constraints limit the user to positioning a single camera and prevent the user from incorporating sophisticated 3D scanning or sensor technology.

The remainder of the paper is organized as follows: Section 2 provides an overview of related work. Sec-

tion 3 outlines the system pipeline of our visualization system. Section 4 briefly describes the reconstruction technique we follow, and detail our method for extracting error sensitivity from single camera. Section 5 gives the design process for visualizing multiple error sensitivity and the steps for generating both 2D and 3D error visualization. Section 6 and 7 gives an evaluation of our proposed visualization scheme and how this meets our requirements. Feedback from end-users and domain experts is used to evaluate our visual mappings of multiple error sensitivity and to discuss the usability of the system. Finally, Section 8 concludes the work.

2 Related Work

The key themes from the literature that this paper concentrates on are: multi-field visualization and uncertainty visualization. The following section discusses the related work from each of these topics.

Multi-field Visualization: Geometric shapes are often used to represent multiple data attributes. Barr [3] presents such an approach by introducing primitives (superquadrics) used for creating and simulating three-dimensional scenes. Shaw *et al.* [33] describe an interactive glyph-based framework to visualize multi-dimensional data using superquadrics which then Kindlmann [17] extends further to visualize tensor fields.

An alternate approach for representing multi-field data is to overlay multiple visualizations onto a single image. Crawfis and Allison [11] introduce a novel approach to achieve this using texture mapping and raster operations. Kirby *et al.* [18] stochastically arrange multiple visualization layers to minimize overlap, to provide greater emphasis to higher layers. Taylor [34] provides an overview of techniques for overlaying scalar fields onto the same surface, and evaluates their performance. More recently, Kehrer *et. al.* [16] describes the importance of visualizing data with multiple parts in scientific simulation, and demonstrate this using an interactive brushing application.

Uncertainty Visualization: Many approaches have been used to quantify and visualize uncertainty. In particular, glyphs [40,22] are well suited for illustrating uncertainty in vector fields where data properties such as direction, magnitude can be mapped to length, area, color and/or angles. Botchen *et al.* [5] introduce a method to visualize uncertainty in texture-based flow fields, by using a convolution filter to smear out probability-based particle traces.

Other methods include procedural annotations [8] to show uncertainty information simultaneously with the data while minimizing visual distraction. Pang *et al.* [28] and Verma and Pang [38] present comparative visualization tools to analyze differences between vector datasets represented as polylines. Brown [7] demonstrates the use of vibrations to visualize data uncertainty, by investigating oscillations in vertex displacement and changes in luminance and hue. Sanyal *et al.* [32] illustrate uncertainty in numerical weather models using glyphs, ribbons and spaghetti plots.

3D Reconstruction: A comprehensive overview for performing 3D reconstruction is described by Hartley and Zisserman [15]. Our technique is based on the work by Legg *et al.* [21] for single-camera reconstruction of a snooker scene using projective transformation given any arbitrary table view.

For evaluating 3D reconstruction errors, various methods have been proposed in the past decade. The work of Weng *et al.* [39] is one of the earliest instances of estimating the standard deviation of reconstruction error using first order perturbations in the input. Broida and Chellappa [6] derived the Cramer-Rao lower bounds (CRLB) on the estimation error variance of the structure and motion parameters from a sequence of monocular images. Zhang [42] presents an important contribution on determining the uncertainty in the estimation of the fundamental matrix. Finally, Morris, Kanatani and Kanade [25] extend the covariance-based uncertainty analysis for the geometric indeterminacies like scale change.

Sensor Planning: Sensor planning typically operates on a pre-defined selection of sampling points centered around the object of interest. Cowan and Kovesi [10] present automatic sensor placement based on optimizing the sensor resolution, focus, field of view and visibility to reduce the cost of vision applications. Examples may include planning of the Next Best Pose (NBP) [41] and object reconstruction [2]. MacKinnon *et al.* [23] introduce quality metrics to improve laser range scanning by minimizing data acquisition. The authors recognise that quality metrics often ignore physical properties and sensor limitations. To the best of our knowledge, this is the first paper to address uncertainty associated with multiple error-sensitivity fields as a result of camera positioning for 3D scene reconstruction in conjunction with other constraints (e.g., physical, financial) for optimal camera placement.

Viewpoint Selection: Previous work has been carried out for addressing different types of viewpoint selection problems. In visualization and computer graphics, several methods have been proposed towards se-
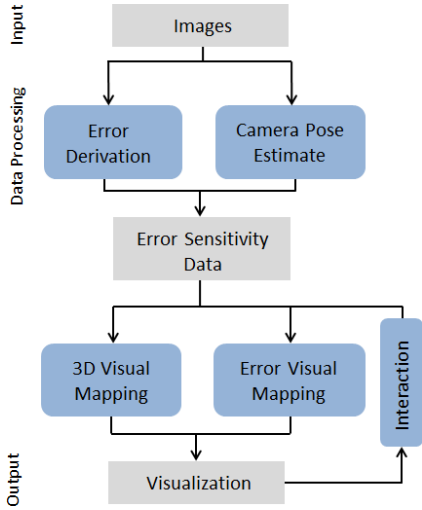
Fig. 2 An overview of the combined visualization pipeline for depicting error sensitivity in single camera positioning. There are three main stages: Extracting the error sensitivity data from sample camera positions, generating the 2D error map and generating the 3D environment visualization.

lecting a (virtual) camera for obtaining the most information viewable to a user for scene understanding [37], volume visualization [4] and image-based modelling [19, 12]. Other types of camera positioning problems include vision-based approaches [10] for achieving a (non-restricted) viewpoint that reduces the cost of vision applications. Our problem follows the latter. However, the application in our case differs in that we include additional physical and financial constraints. Not all viewpoints are possible. We also emphasize that the constraints in our applications are dynamic, making direct encoding non-feasible.

3 System Overview

The system comprises of three key aspects: extracting the error sensitivity data, generating the 2D error map and generating the 3D environment visualization. An overview of the system is shown in Fig. 2. The first stage involves taking a set of sample images from given camera positions around the scene as shown in Fig. 3. We extract the associated error-sensitivity fields which is detailed in Section 4. Following this, we estimate the camera pose from each image which is necessary for mapping the camera position to the 3D environment.

The second stage maps the corresponding error sensitivity fields using visual designs we propose in Section 5. This aids the user in analyzing the uncertainty at given positions and allows a visual comparison of multiple cameras. In the final stage, a 3D visualization is generated to summarize multiple error sensitivity associated with each camera and to incorporate contex-


Fig. 3 A 3D reconstruction of the camera environment in the snooker scene. A set of sampled camera positions are shown using grey spherical markers around the region of interest.

tual information about the scene. Each visualization is displayed simultaneously or on a dual-screen, allowing the user to interact with the 3D visualization whilst analyzing the error sensitivity in detail. Sample camera positions can be selected within the environment which update the error map visualization accordingly. In addition, users can filter cameras based on error-sensitivity to highlight potential camera suggestions.

4 Camera Sensitivity and Error Derivation

Three-dimensional reconstruction and object tracking are highly sensitive to camera placement. Many systems (e.g., *Hawk-eye* [26]) adopt multiple cameras to overcome problems such as object occlusion and sampling errors. The Hawk-eye ball tracking system is commercially used in sports such as Tennis, Snooker and Cricket to accurately reconstruct shots for television broadcasting. It is vital that the images captured from each camera contain sufficient information about the scene. There are many factors in camera sensitivity that will affect the image quality used for reconstruction:

- *Resolution* — the physical size of the image captured by the camera determines the amount of sampling error of the image data.
- *Viewing Angle* — the maximum angle in which a display can be viewed. This highly affects the avail-
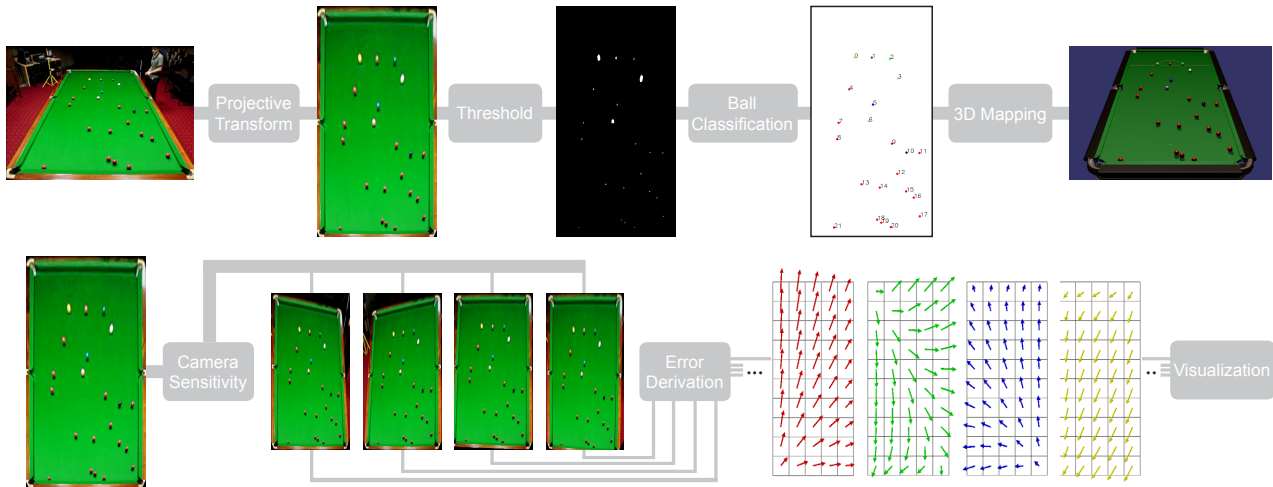
Fig. 4 (Top) Reconstruction pipeline for extracting ball positions in a snooker scene using a single camera. The 3D reconstruction is based on a 2D homography. (Bottom) Camera sensitivity analysis of the projective transform. Error sensitivity fields (or vector fields) are derived to quantify the impact of image distortion from inaccurate feature correspondence.

ability and selection of camera poses (see below) that fully capture the entire scene.

- *Camera Pose* — is a combination of position and orientation of the camera with respect to a static object in the scene.
- *Lighting Condition* — lighting variance can affect processing steps such as color classification.
- *Camera Vibration* — the stability of the camera should be minimized to reduce errors in feature detection.

In our case study, we focus on using 3D reconstruction as part of a coaching tool [20], where only an approximate estimation of the balls is required. Whilst there are key advantages to a multi-camera system, it also presents several practical drawbacks. For instance, such a system needs to be manually calibrated before use. This step can often be overwhelming and time consuming to a novice user such as snooker coaches and players. More significantly, snooker clubs and academies have yet to benefit from such technology due to the cost of installation (e.g., around £200,000 for Hawk-eye). To facilitate our target users, we propose error analysis on a more flexible system using a single camera [21]. One desirable ability is to review a sequence of training shots [29] to support performance analysis. In order to perform ball tracking, we use a high-speed ethernet camera capturing at 200 frames per second. Since the camera has a fixed resolution, viewing angle, and focal length, our focus is to assess the quality of an image at various camera positions that give the most reliable reconstruction.

4.1 Snooker Reconstruction

The goal of snooker reconstruction is to estimate the spatial position of the snooker balls. As the balls lie along a planar surface, this simplifies the problem to extracting the 2D position (x, y) of the ball object, which can then be mapped onto its 3D model. Guo and Namee [14] were the first to introduce ball reconstruction based on a single, top-down view of the table. We follow the method presented by Legg *et al.* [21], which extends the previous technique [14] to an arbitrary camera position. Fig. 4 (top) outlines this process. The first step involves transforming the image into a top-down view using 2D homography. The next step involves applying a threshold filter to extract the specular highlight on the ball, and approximate the location of each ball. We then identify a full or partial set of balls (e.g., for training shots) using connected component analysis and color classification in the resulting image. In the final step, the extracted balls are mapped to their corresponding position in the 3D model.

Fundamentally, the reconstruction accuracy of the balls is determined by the camera position that gives the least amount of projective error. In an ideal scenario, a camera would be placed directly top-down above the table. However, in snooker and many other sporting facilities (e.g., table tennis and pool), constraints such as lighting fixtures, the cost of mounting the camera and the practicalities of the camera position (see Fig. 1 for an example) means this is not possible. Therefore, we need to find alternative solutions. We determine the quality of an image by evaluating the error sensitivity of the 2D homography associated with each camera pose.
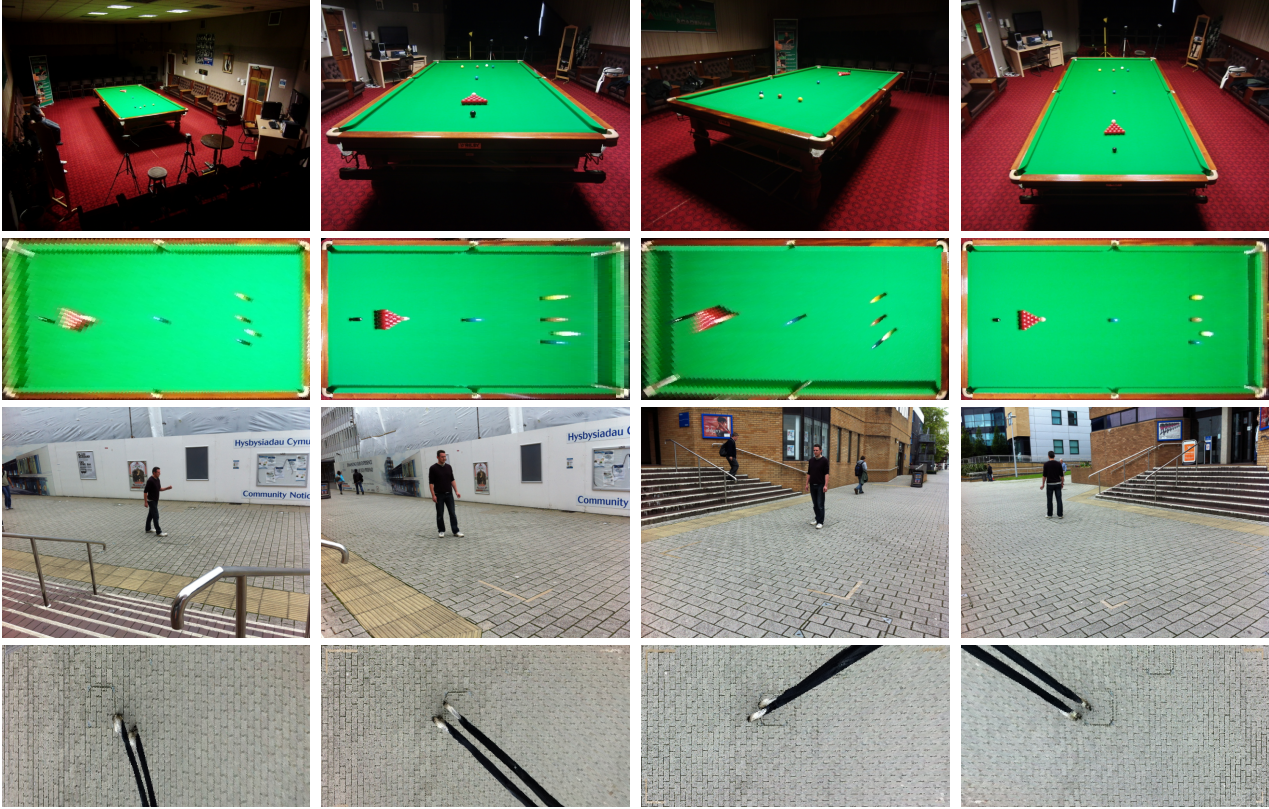
Fig. 5 Example camera positions around the (First row) snooker table scene and (Third row) security scene. Below each image is the associated inverse transformation of the camera position to obtain a top-down table view. It can be seen that the quality of the inverse transformation is greatly influenced by the camera position.

4.2 Homography Sensitivity Analysis

Homography in vision-based applications [15] is used to describe the projective mapping of a set of coplanar feature points $\mathbf{a}_i \in \mathbb{R}^2$ in the observed scene onto another set of coplanar points $\mathbf{b}_i \in \mathbb{R}^3$ in the model. Algebraically, corresponding tuples of points are related to each other by $\mathbf{b}_i = \mathbf{H}\mathbf{a}_i$ where the 2D homography $\mathbf{H}$ is a 3x3 matrix. Errors in the transformation are typically introduced in the detection of feature points $\mathbf{a}_i$, as well as in the correspondence procedure. The impact of noise in the image, visual artifacts and even camera vibration can lead to false detection. In addition, we find that the stability of homography parameters are greatly affected depending on the camera pose (see Fig. 5 for examples). Therefore, to investigate the quality of different camera positions, we assess the sensitivity of feature points for homography estimation. This is illustrated graphically in Fig. 4 (bottom).

Suppose for an image I, we have a set of known ground truth positions of feature points $\mathbf{a}_i$ that are mapped onto a set of coplanar points $\mathbf{b}_i$ in the model for $i = 1, \ldots, N$. The solution to $\mathbf{H}$ will give an accurate projective mapping from one plane to the other. Now let $\delta\mathbf{a}_i \in \mathbb{R}^2$ be a noisy feature point imposed by some fixed

deviation within a sensitivity region $dist(\mathbf{a}_i, \delta\mathbf{a}_i) \leq r$, for $r \in \mathbb{R}$. Analytically, errors under the new homography mapping $\mathbf{H}'$ can be shown using the displacement vector $\underline{\delta\mathbf{b}} = \mathbf{H}\underline{\mathbf{a}} - \mathbf{H}'\underline{\mathbf{a}}$, where $\underline{\delta\mathbf{b}} = \{\delta\mathbf{b}_i\}$ represents the projective error when a set of points $\underline{\mathbf{a}} = \{\mathbf{a}_i\}$ is mapped onto the new plane. In image space, we describe the error in 2D homography as a set of 2D vector fields $\mathbf{D}^{(i)} : \mathbb{R}^2 \mapsto \mathbb{R}^2$:

$$\mathbf{D}^{(i)}(x,y) = \mathbf{H}(x,y) - \mathbf{H}^{(i)}(x,y) \tag{1}$$

where $\mathbf{H}^{(i)}$ denotes the set of erroneous homographies corresponding to the sensitivity of each feature point $\delta\mathbf{a}_i, \ldots, \delta\mathbf{a}_N$. Any inaccuracies in feature point correspondence will greatly affect the visual quality of the projective transformation. The 2D vector fields are used to effectively depict the amount of distortion as shown in Fig. 4 (bottom). Typically, one may combine multiple error sensitivity fields to illustrate the uncertainty associated with one or several feature points. Hence, we can generalize planar error sensitivity using m 2D error fields, where $m \geq N$. The resultant error field $\gamma : \mathbb{R}^2 \mapsto \mathbb{R}^2$ caused by each field is one example used to provide a statistical overview. This can be computed explicitly by Eq 1, or implicitly using the summation:

$$\gamma(x,y) = \sum_{1}^{N} \mathbf{D}^{(i)}(x,y) \qquad (2)$$

Due to the non-uniform distribution of errors, we find that the compositional effects of multiple error fields can lead to the negation of uncertainty. We refer to this as *vector cancellation*. This can be shown using the subadditivity property inherent in our function. Let $\mathbf{d}_i = (\mathbf{d}_{x,i}, \mathbf{d}_{y,i})^T \in \mathbf{D}^{(i)}$ be the displacement vectors for each field and $\lambda = (\lambda_{x,i}, \lambda_{y,i})^T \in \gamma$ denote the resultant vector at a fixed point, it holds that:

$$||\lambda|| = ||\mathbf{d}_1 + \ldots + \mathbf{d}_N|| \leq ||\mathbf{d}_1|| + \ldots + ||\mathbf{d}_N|| \qquad (3)$$

Hence, the worst case of cancellation occurs when $||\lambda|| = 0$ whilst $\exists \mathbf{d_i} \in \mathbf{D}^{(i)}$ such that $||\mathbf{d}_i|| > 0$ for $i = 1, 2, \ldots, N$. It is possible to take this error into account using absolute vectors or sum of vector magnitudes. However, as a result we lose other information (e.g., direction) that is critical in the analysis of planar error sensitivity. This includes identifying sensitive parameters and using the distribution of errors to guide optimization algorithms. Hence, we find it becomes advantageous to visualize multiple error fields.

In our applications, we rely on detecting four feature points. For snooker, these points are defined by the table boundaries, where the focus is to obtain absolute ball positions for 3D scene reconstruction. In video surveillance, we use the corners of a marked rectangular region in which the position of pedestrians is of importance for vision-based applications. Using a sensitivity region of $r = 20$, we develop visual methods for depicting the four error sensitivity fields as a means for assessing camera sensitivity.

5 Error Sensitivity Visualization

We propose an interactive visualization system for planning the optimal positioning of a single camera based on error sensitivity and various physical and semantic constraints by allowing the user to incorporate their knowledge into the decision process. The visualization consists of two components: 1) a 2D visual map for depicting the compositional effects of multiple error sensitivity fields for each camera, and 2) a 3D visualization scene to illustrate the environment in which the camera configuration is to be arranged, adding context to the user. The 3D visualization allows the user to investigate the feasibility of camera positions based on environmental constraints and gives an overview of the error sensitivity associated with each camera. We support user exploration through an interactively linked 2D error mapping, and provide user options for filtering and displaying specific camera samples (e.g., with lowest error sensitivity) in a focus+context manner. In this Section, we outline some design considerations largely based on [35] in order to deliver effective visualization. We then detail our design process for the visualization of multiple error sensitivity fields extracted from camera sensitivity analysis (see Section 4), and describe a method for estimating the camera pose for mapping sample camera points to a 3D environment. Finally, we present our method for integrating error sensitivity into the 3D environment using a spherical visualization.

5.1 General Design Principles

We shall concentrate primarily on multi-field data visualization, however these design principles are applicable to other areas of visualization also. To ensure suitability of the sensitivity visualization, we outline the essential requirements that the visualization must conform to:

– **R1. Detail** — the visualization needs to clearly depict multiple error fields, each of which is a 2D vector field obtained from a single camera or from multiple cameras.
– **R2. Overview** — the visualization needs to show a summary overview that illustrates the combination of error sensitivity fields in a given contextual geometry.
– **R3. Cancellation** — the visualization needs to represent uncertainty cancellation that may be present as a result of error field composition.

In addition to this, we want to ensure that the visualizations proposed are simple and intuitive in their formation. We consider a number of design principles that aim to enhance the quality of the visualization for conveying useful information to the user.

Visual Simplicity The focus of the visualization should be to convey the contents of data and to allow for user exploration, as opposed to the visualization technique itself. For higher-dimensional scenarios this can often be conceptually difficult and hence a more complex representation is required. We present a range of visual designs with varying degrees of complexity ranging from simple color-maps to multi-attribute glyphs. Additionally, we combine and make use of existing techniques (e.g., heat maps, vector glyphs and streamlines) that are familiar in the domain to support learnability of our visualization.

(a) Vector Glyphs

(b) Co-Planar Star Glyphs

(c) Stacked Ribbon and Streamlines

(d) Bezier Glyphs
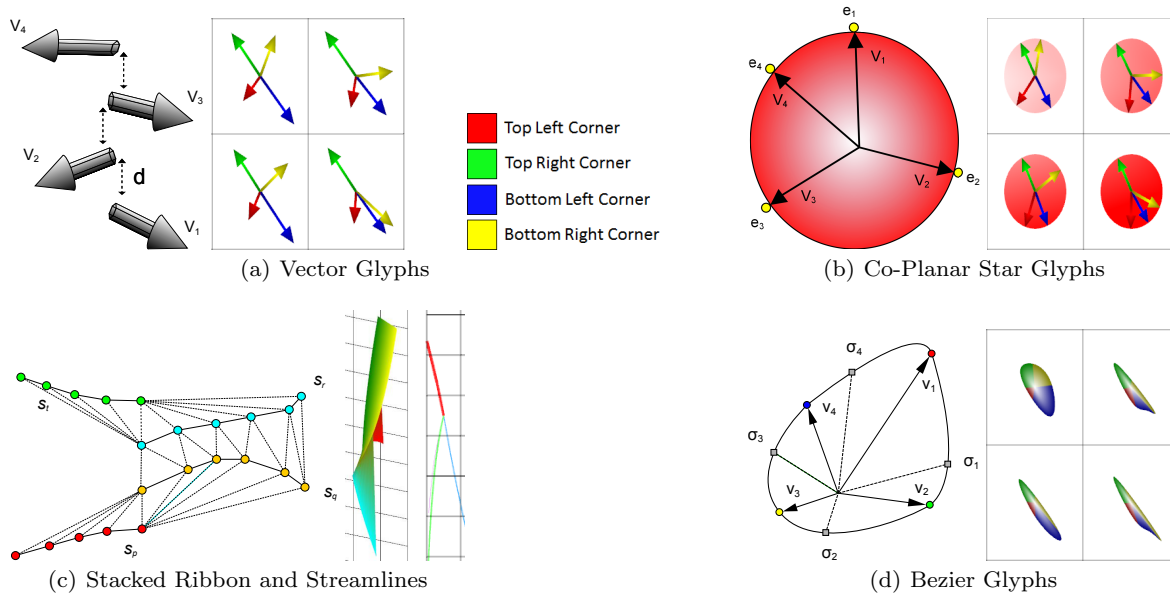
Fig. 6 Development of the 2D error visualization using different approaches is shown. (a) presents a stacked vector glyph design, where magnitude is mapped to the length of the vector. This is extended in (b) to a Co-Planar Star glyph which normalizes the vectors and uses a heat map to depict the resultant error. (c) incorporates stacked ribbons (center) and streamlines (right) into the error visualization. Streamline thickness is mapped to vector magnitude. (d) generates a closed Beziér curve based on the vector field. The glyph size is mapped to the resultant error.

Visual Comparison In order to promote effective decision making, it is essential that visualizations can be perceptually evaluated and that comparisons can be made between two representations. By making visualization more comparative, a user should be able to visually rank two given data sets based on their visual representations. We have designed visualizations that allow the observer to compare camera positions and their associated error (e.g., Fig. 9).

Relationships Between Data Attributes One of the main advantages of visualization is that it provides greater insight into the underlying phenomena. In the case of multivariate data, we are particularly interested in how different attributes affect one another and these relationships should be conveyed to the viewer. Our multi-attribute glyphs enable the user to examine the relationships between multiple error-fields. For example, our Beziér glyph integrates multiple vector attributes into a single shape that allows the user to perceive the distribution of error more easily.

Integrity Misleading visualizations are common [13]. Principles tuned towards statistical graphics can provide suggestions that help limit unintentional visualization lies. For instance, clear labelling should be used to help users overcome graphical ambiguity (e.g., Fig. 8).

The aim of multi-field visualization is the depiction of multiple fields that are co-located in the same do-

main for revealing complex interactions that occur between fields. Simulation data is one example where several fields (e.g., pressure and temperature) and associated uncertainties are studied together to make accurate predictions. Thus, the challenge is to make a coherent visualization that is meaningful given the high-dimensionality of the data. It is possible using statistical functions such as vector magnitude to simplify the input data and encapsulate the phenomena into a single field. However, as a result we lose information (i.e., vector direction) which may be necessary in the analysis. Therefore, we strive towards visualizing multiple fields to provide greater insight.

5.2 Visual Mapping of Multiple Error Sensitivity

The visualization of multiple error sensitivity fields is important for making comparative assessment between different camera positions. Understanding the distribution of error is an important task to support various user-specific needs. For example, the action from a snooker training shot may typically cover a small region of the table. Therefore, camera positions that minimize the error in this area should be considered in addition to camera positions that has least, overall error sensitivity. The knowledge gained from each field can be used to minimize the reconstruction error further (e.g., as a optional post-calibration step) by optimizing sensitive feature points that impact this region. It would be a

huge challenge, if not an impossible one, to provide a visual design for an arbitrarily large number of fields. Here we consider a collection of visual designs for four error sensitivity fields which is minimal for solving planar homography matrix, addressing the requirements of our case studies. Fig. 6 shows five example approaches that have been considered for the design of the visualization: Vector Glyphs, Co-Planar Star Glyphs, Stacked Ribbon and Streamlines, and Bézier Glyphs.

Vector Glyphs: Arrow primitives is the most common method for depicting vector quantities. As a naive approach, we use four color-coded arrows for representing each of the vector fields at a given point (Fig. 6(a)). The length of the arrow is mapped according to the error magnitude with respect to each field. For visualization, the vector glyphs can be rendered either on the same plane (i.e., for $d = 0$), or separated so that each individual vector field is rendered on an independent plane, resulting in four layers in 3D space. This aims to overcome overlapping issues that may arise.

Co-Planar Star Glyphs: Due to inevitable overlapping problems with vector glyph representation in dense sampling, the directional information can often be lost. To reduce glyph occlusion and preserve vector direction, the star glyph uses four normalized color-coded arrows. However, rather than using arrow length to indicate vector strength we now use colored transparent ellipses (Fig. 6(b)). The four points on the ellipse e_1, e_2, e_3, e_4 are used to map a gradient to the circle based on error magnitude for each vector. This creates a heat map which is effective for highlighting regions of large error.

Stacked Ribbons / Streamlines: Streamlines are an effective and well-known technique for visualizing vector fields [24]. Urness *et al.* [36] present several strategies for visualising two vector fields. We adopt their streamline approach for our error visualization by mapping curve thickness to error magnitude (Fig. 6(c)). Just as was found using vector glyphs, there are instances where occlusion can occur meaning that the vector fields can not be displayed clearly. For a more continuous representation, we extend streamlines to 3D space by rendering each vector field on a seperate plane. A surface is used to connect streamlines on adjacent planes, resulting in a stacked ribbon.

Bézier Glyphs: Our approach considers the vectors as a series of points that form a closed Bézier curve (Fig. 6(d)). This preserves the directional information that the vector glyphs offer, whilst giving greater visual clarity to the extreme directions of the four vector fields. The parametrized Bézier curves are divided into regions using distribution points σ_i centered at the mid-

point of each spline, which adaptively move along the curve based on the difference in vector strength:

$$\sigma_i = \frac{1}{2}\left(1 + \frac{||\mathbf{v}_i|| - ||\mathbf{v}_{i+1}||}{\max(||\mathbf{v}_i||, ||\mathbf{v}_{i+1}||)}\right) \tag{4}$$

where $\mathbf{v}_i$ and $\mathbf{v}_{i+1}$ are two adjacent vectors. This allows the user to identify which error source (i.e., vector field) is of dominant influence to the resulting geometrical shape of the Bézier glyph.

5.3 Sample points in 3D visualization

To introduce camera positions into the 3D scene visualization, we determine the geometry of the table to obtain a camera pose estimate. Given that we have four feature points and their corresponding positions in a 3D model, it is possible to estimate the viewing angles from a single image. Here we use the four corner points of the snooker table. The basic scheme is detailed by Putz and Zagar [30], where a planar homographic transformation matrix is computed and an SVD-based approach is applied to extract the rotation and incline angles. A mapping function is applied to render the cameras in 3D space using the camera pose and the measured camera distance. In addition, filtering can be applied to highlight the k-least error camera positions. We use a similarity metric d based on euclidean distance to provide k spatially different solutions to the user.

5.4 Spherical Mapping

Now that we can map our camera points to the scene, we use a spherical model to give an overview of the error sensitivity of such positions (see Fig. 7). We visualize camera positions using spherical markers and a connecting cylinder with length being mapped to the distance between the camera, and the sphere that encloses the focus region. A spherical geometry was chosen due to its uniform characteristics and its potential to be generalizable to other domains. Here, we use a partial spherical mesh to emphasize the boundary of camera positions. To quantify each camera, we propose two visual options: multi-field glyphs and color-coded sphere. For our glyph-based method, an average Bézier glyph representing the multiple error sensitivity fields are placed tangental to the sphere. For a color-coded sphere, we depict the summation of the resultant error sensitivity field normalized by $\frac{\epsilon}{\epsilon_{max}}$ using a red-to-blue color mapping. The vectors (or error magnitude) are splatted onto the sphere using a gaussian weighted Radial Basis Function (RBF) [9] forming an interpolated
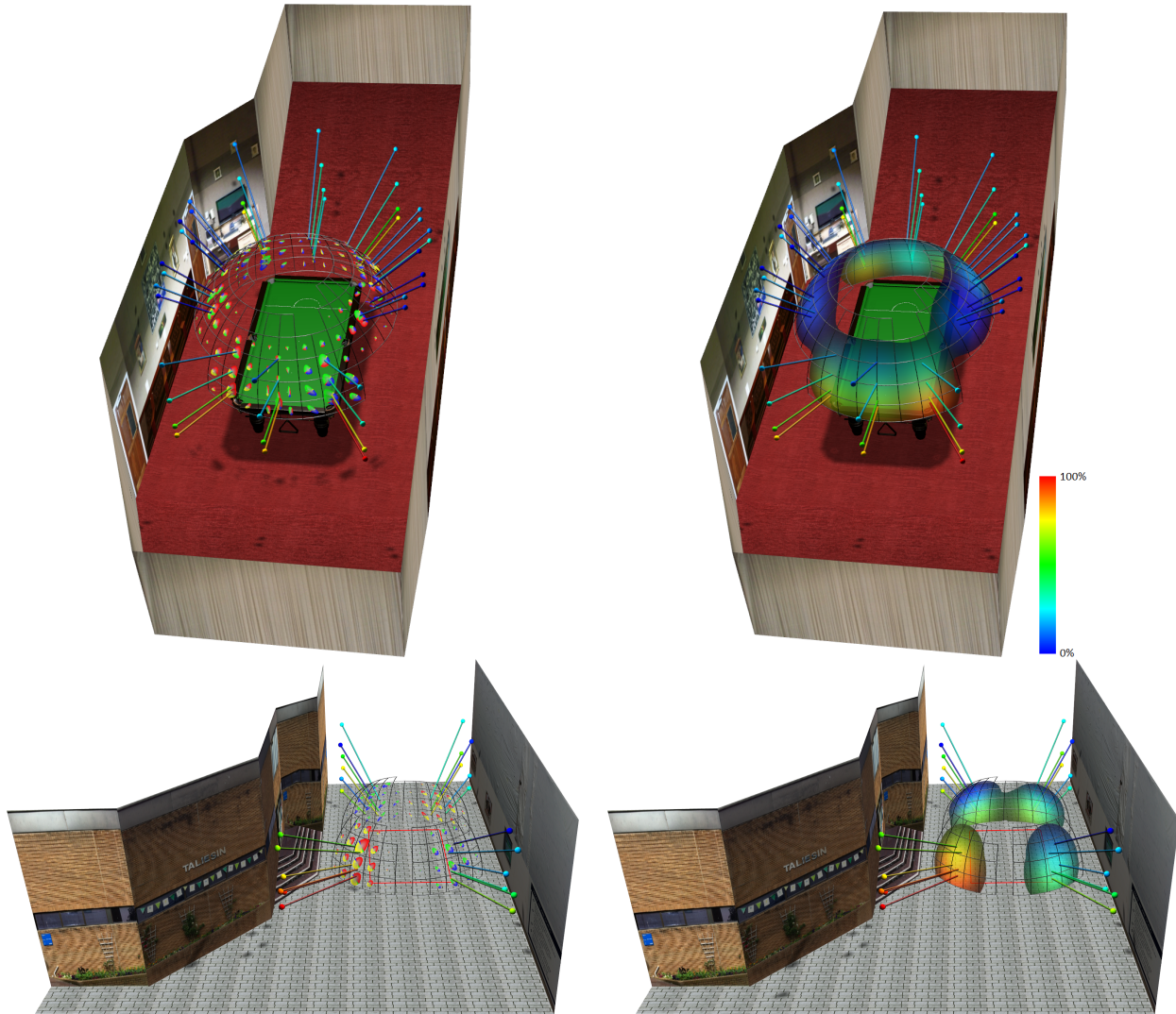
Fig. 7 Visualization showing the 3D camera positioning around the snooker scene (Top row) and security scene (Bottom Row). The cameras are modelled using spheres which are color mapped to error magnitude. The sample points are then projected onto spherical co-ordinates centered at the focus region, giving users a uniform overview of the statistical error. (Left) shows a glyph-based approach for depicting the average vector error and (Right) uses a color-mapped sphere for illustrating the overall error magnitude.

surface that gives visual estimates of local regions. We uniformly position the glyphs along the surface of the spherical mesh. Each point on the sphere is modeled as:

$$v(q) = \sum_{i}^{n} w(\mathbf{q}, \mathbf{p}_i, r) v(\mathbf{p}_i) \qquad (5)$$

where $v(\mathbf{q})$ is the camera error at position q, and $w(\mathbf{q}, \mathbf{p}_i, r)$ is the RBF weight function given by:
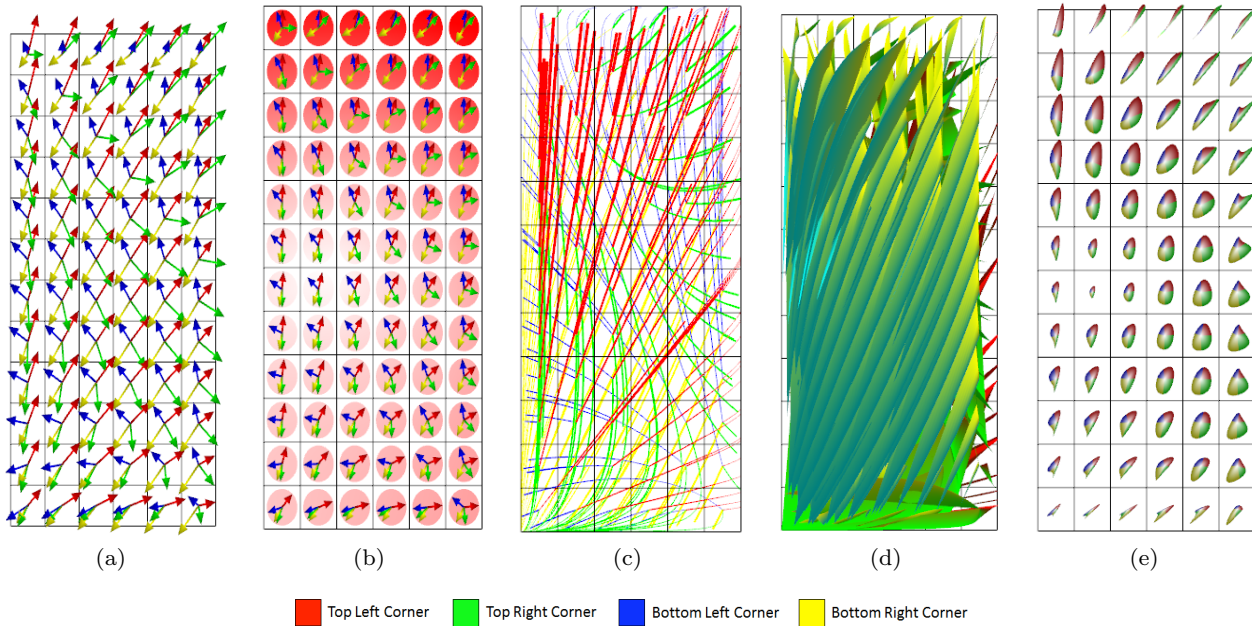
$$w(\mathbf{q}, \mathbf{p}_i, r) = e^{-\beta u_i^2} \qquad (6)$$

where $u_i = ||\mathbf{q} - \mathbf{p}_i||/r$ is the relative distance from $\mathbf{q}$ to $\mathbf{p}_i$ normalized by the radius of influence r, for some $\beta > 0$.

Naturally, the RBF tends towards zero as the distance tends to infinity and hence a restriction is placed on the kernel based on the radius of influence. The user option β, is a coefficient that can be altered in order to adjust the slope of the blending function.

6 User Consultation - 2D

We have proposed 2D and 3D visualization methods to depict the error sensitivity in 3D scene reconstruction for estimating optimal camera placement. It is essential that the visualizations can effectively convey to the user the presence of error and to allow visual and comparative analysis of different camera positions. To evaluate the effectiveness of our designs, we perform a qualtita-

(a)   (b)   (c)   (d)   (e)

■ Top Left Corner   ■ Top Right Corner   ■ Bottom Left Corner   ■ Bottom Right Corner

Fig. 8 Comparative evaluation of error visualization designs. (a) uses stacked vector glyphs. (b) co-planar star glyphs. (c) weighted streamlines. (d) stacked stream ribbons and (e) color-coded Bézier glyphs.

| Design criteria:	Visual Designs (Fig. 8)				
	(a)	(b)	(c)	(d)	(e)
Independent vector direction	*	*	*		*
Independent vector magnitude	*				*
Overall error		*			*
Error distribution					*
Visual separation of fields			*		*
Vector cancellation					*

Table 1 Comparison of visual mappings shown in Fig. 8. Each design is assessed against a number of set criteria which ideally should be achieved. An asterisk in the table indicates the design satisfies that particular criteria.

tive user-evaluation involving six computer scientists, three of whom are experts in computer vision. Fig. 8 shows the collection of error-sensitivity mappings of the same camera position using the five visual designs in Section 5.2. Each study was carried out independently from one another, whereby participants were presented with a set of questions (see Appendix A) which we classify into three groups: *Detail, Overview* and *Cancellation* derived from Section 5.1. The remaining questions provide more general observations in order to evaluate whether our visualization approach is useful for the given task.

R1. Detail: It is important that multiple error-sensitivity fields can be visualized within a single image. To start with, we asked the users whether they can identify the independent vector magnitude and directions at a given point for each of the visual designs. Whilst four of the five designs succeed to perform the basic functionality of conveying detail, some designs have limitations. It is clear from the evaluation study that the

use of stream ribbons (Fig. 8(d)) for depicting multiple error fields over several planes created too much visual clutter and occlusion. As a result, the users found the information to be lost. Viewpoint adjustment may overcome this, however it cannot be guaranteed. Whilst not quite so severe, we found that Figures 8(a) and 8(b) may also suffer from occlusion issues should two vectors have the same direction and magnitude. Although both magnitude and direction are visible in our streamline approach as shown in Fig. 8(c), there were questions raised over the accuracy of comparing thicknesses between two streamlines in a quantitative manner. All the users found the Bézier glyphs (Fig. 8(e)) to be most effective in conveying both attributes but revealed that independent vector direction became difficult to perceive for elongated glyphs (i.e., when vectors are in the same direction).

R2. Overview: In many focus and context visualizations, it is necessary to show the overall sensitivity for multiple fields, whether this be introduced by one or multiple cameras. The overall sensitivity can be assessed based on two uncertainty components, the overall error (resultant magnitude) and the distribution of error from each error sensitivity field. In Fig. 8(a), although the overall error is not explicitly mapped, users were able to estimate the error given by the four vectors. However, the presence of visual clutter likewise in Fig. 8(c) and 8(d) made this difficult to deduce easily. Fig. 8(b) performed significantly better by mapping the overall error from multiple fields using intensity. The heat map behind the glyph is effective for estimating
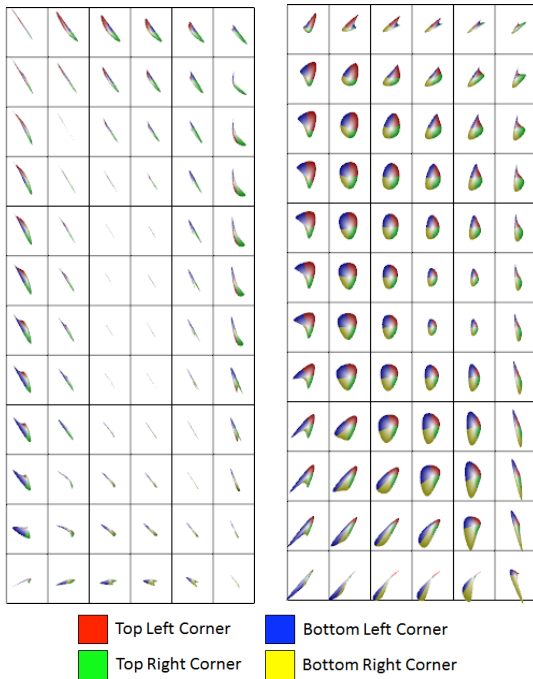
Fig. 9 Comparison of error sensitivity between camera positions B (left) and position C (right) from Fig. 11 using color-coded Bézier glyphs.

local regions of uncertainty. One limitation with the design is that visual interference were found to occur between the vector fields and the heat map. Fig. 8(e) also shows the overall error from multiple fields, this time by size. The larger the Bézier glyph appears determines the amount of error at the location. Most of the users acknowledged this design to be the most intuitive and descriptive when displaying error, stating that the glyph shape provides a visual cue that is clearer for error analysis.

One of the goals of multi-field visualization is to be able to observe each field independently, whilst providing additional insight on how multiple fields interact. We found that vector-glyph based designs performed weakly at this task due to visual clutter, with users stating it was difficult to visually integrate between fields. On the otherhand, the streamline visualization performed particularly well due to its continuous representation. The color segments in the Bézier glyphs were also effective for visually seperating error fields, but these became lost for highly elongated glyphs.

R3. Cancellation: Fig. 8(e) is the only visualization to truly incorporate this requirement. This is determined based on the shape of the Bézier glyph. A circular glyph would indicate a high level of vector cancellation from multiple fields. However, any skew or elongation would represent dominant vector direction that is influencing the error for that position. It is possible to
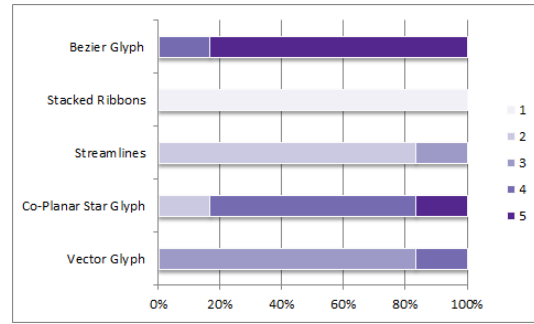

Fig. 10 Graph showing the result of users ranking the visual designs from worst-to-best as a measure from 1-5.

estimate cancellation from Figures 8(a) and 8(b) if two vectors are recognized to be in opposing direction, however only the Bézier design actually incorporates this. Table 1 provides an overview of the performance for each visual design.

In the study, we asked the participants whether the visualization approach would assist in visually quantifying a camera position based on uncertainty. The feedback was positive and the users expressed the distribution of error shown by the visualization would help attach a weighting to a particular position. One computer-vision expert in the study revealed that the depicted error distribution could be used for optimizing vision-based tasks such as correcting more sensitive feature points. Another participant noted the visualization is useful for revealing camera positions with symmetric reprojection error.

Fig. 9 gives the error mapping for two different camera positions. This provides visual comparison of the error senstivity that is present from each camera viewpoint. By analyzing the changes between the Bézier glyph representation based on size, shape and color, the user can determine the viewpoint that reduces the impact of error. Following the study, all users found the visualization approach to significantly help evaluate viewpoints based on error-sensitivity in a comparative manner. From this example, camera position C experiences large error that is significantly reduced in camera position B. Lastly, Fig. 10 shows the results of the users preference by ranking the visual designs from worst-to-best. Results from the study show that users felt the Bézier design to be the most intuitive and effective in conveying error sensitivity. In the remainder of this paper, we use the Bézier design during the user evaluation of the software which combines both 2D and 3D visualizations for finding an optimal camera position.
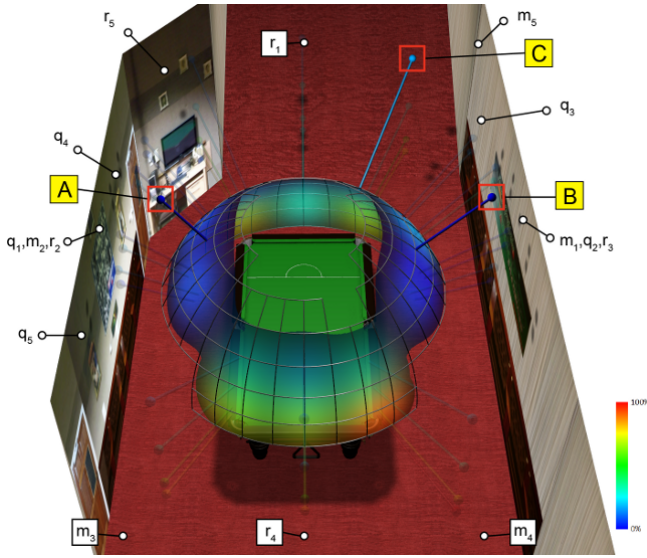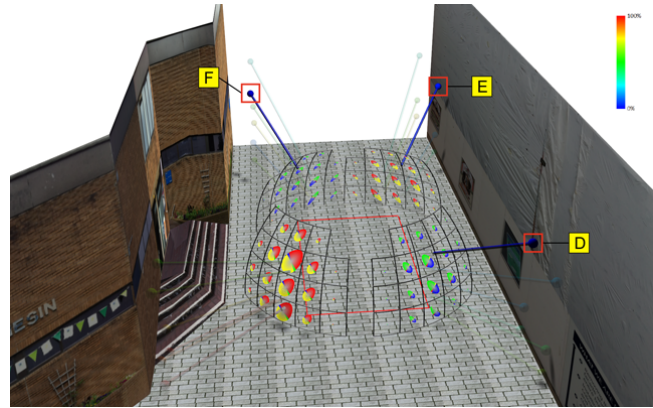
Fig. 11 3D visualization showing the 3 candidate camera positions labelled A, B and C, after filtering. These camera positions are highlighted using opacity.

Fig. 12 3D visualization showing the 3 candidate camera positions in the surveillance scene labelled D, E and F after filtering. These camera positions are highlighted using opacity.

7 User Consultation - 3D

To evaluate our combined visualization system for selecting an optimal camera position, we conducted a study using two sets of users: three sport scientists, and three computer vision experts. We use this study to compare and contrast the decision process between end-users with minimal reconstruction knowledge using our visualization approach, and domain experts in the field of computer vision without error analysis support. Each study was conducted in isolation from other participants so not to influence the given opinions.

Our first study involved three sport domain experts: A snooker coach and former world champion, a snooker hardware engineer and a sports scientist. We started by explaining the motivation behind the work to each participant. It was made clear that given a single camera to configure, we wanted the position that would achieve accurate reconstruction and is most feasible for installation (i.e., taking into account physical, financial and other types of constraints). We note that the users have some prior knowledge of the scene such as structural information of the room and cost of mounting equipment which they can incorporate into the decision. Fig. 7 was presented where they were asked to give their feedback on the usability of such a visualization. The initial reaction was very positive by all three participants. In particular, they were able to quickly identify potential camera positions, namely above the left and right hand side of the snooker table. We explained to each participant how a user can filter the number of cameras based on error sensitivity to highlight candidate positioning. Fig. 11 shows the result of the user filtering down the

data to just three prospective camera positions. This helped validate the users' understanding of the visualization as two of the three positions matched their initial observations.

The next objective was to assess how well the visualization integrates contextual geometry to influence the decision process. By navigating in the virtual environment, the feedback received suggested that the camera should be positioned to the right of the table. Participants recognized that both this and the position left of table were the two best choices. Through inspection of their error sensitivity maps, the users identified the left camera position (Camera A) to be marginally more accurate. However, due to mounting impracticalities on the left wall such as picture frames and scoreboards, the users realized that camera placement here was not a viable option. The participants found the error visualization to be clear when comparing cameras with significant error variance (see Fig. 9). As a result, the visualization approach proved useful for clarifying the error associated with each camera position. Prior to using the visualization, the hardware engineer assumed that the best camera position would be near the bottom end of the table giving a typical TV broadcasting view. The participant was surprised by the visual results to find that the cameras either side of the snooker table were the least error prone positions, and appreciated that the visualization showed greater insight to the setup procedure for 3D scene reconstruction.

The second study involved the computer vision experts $\mathbf{q}$, $\mathbf{r}$ and $\mathbf{m}$. Initially, each participant was asked to nominate the 5 *best* positions for single camera reconstruction given there were no constraints. A uniform decision was observed, where the camera position directly top-down was identified as optimal. This is to be expected, however the selection is not viable since

the camera position is unable to provide full coverage of the scene due to a low-ceiling. Following this, we investigate how additional knowledge on semantic constraints (e.g., low ceiling, picture frames) and financial constraints (e.g., cost of mounting) would impact their decision on camera positioning. We note that the cost of a ceiling mounted camera is more expensive due to structural issues in this case study. We asked the participants to repeat the initial task with such semantic considerations in mind. The results are shown in Fig. 11 where camera positions marked as $\mathbf{q}_k, \mathbf{r}_k$ and $\mathbf{m}_k$ are ranked from best ($k = 1$) to worst ($k = 5$). It can be observed that the nominated camera positions amongst the participants significantly diverges in the new task. This shows that camera positioning is not as intuitive once multiple real-world constraints are imposed. We presented the vision experts with the system, where they all recognized the mutual benefits of the visualization as it constrains the search space for optimal camera placement to support consistent positioning.

Fig. 12 demonstrates our method for our second use-case scenario on camera surveillance, where three candidate positions have been highlighted after filtering. Here, we use multi field glyphs to provide a greater level of detail for camera error sensitivity in the 3D scene. This allows users to examine crucial information such as independent and combined error distribution and sensitivity of feature points in a global perspective, with the option to see further detail by examining the associated error sensitivity visualizations. Due to temporary construction works along the featured structure to the right of the region of interest, camera placement here would not be optimal. Therefore, the most suitable position would be along the wall near camera F as this provides a more temporally stable solution.

We present a qualitative evaluation based on the feedback of two sets of users. All participants felt that the visualization helped to identify the most suitable camera positioning in a clear and simple manner. It was shown that for end-users, the visualization facilitates dynamic decisions for optimal camera placement which includes substantial trade-offs between reconstruction quality and camera feasability without the need for extensive knowledge in reconstruction. The sporting professionals all stated that they would use this approach if they were to configure a camera set up. For computer vision experts, the visualization proved to be an excellent aid for single camera placement as a result of confining the search space.

8 Conclusion

We described 2D and 3D visualization methods to display error sensitivity fields for feasible, single camera positioning. The collection of visual mappings depict the composition of multiple error sensitivity fields. These map to a 3D visualization where the goal is to visually estimate several optimal positions for the camera. We find that the visualization can effectively aid the estimation of the best camera positioning without the need for a manual configuration through trial and error, while providing the users with sufficient flexibility to make dynamic decisions based on other facts that cannot be encoded easily in an algorithm. In future work we aim to extend our method for visualizing the composite effects of multiple error sensitivity from several cameras to assist in configuring a multi-camera system. This would potentially benefit real-scenarios where a single optimal camera is not achievable, and that two or more cameras can be used in replacement to compensate non-optimal positioning.

References

1. Agarwal, A., Triggs, B.: 3d human pose from silhouettes by relevance vector regression. In: In Proceedings of Computer Vision and Pattern Recognition, pp. 882–888 (2004)
2. Banta, J., Wong, L., Dumont, C., Abidi, M.: A next-best-view system for autonomous 3-d object reconstruction. IEEE Transactions on Systems, Man and Cybernetics, Part A: Systems and Humans **30**(5), 589–598 (2000)
3. Barr, A.H.: Superquadrics and angle-preserving transformations. IEEE Computer Graphics and Applications **1**(1), 11–23 (1981)
4. Bordoloi, U.D., Shen, H.W.: View selection for volume rendering. In: Proceedings of IEEE Visualization, pp. 487–494 (2005)
5. Botchen, R.P., Weiskop, D., Ertl, T.: Texture-based visualization of uncertainty in flow fields. In: IEEE Visualization, pp. 647–654 (2005)
6. Broida, T.J., Chellappa, R.: Performance bounds for estimating three-dimensional motion parameters from a sequence of noisy images. Journal of the Optical Society of America **A6**, 879–889 (1989)
7. Brown, R.A.: Animated visual vibrations as an uncertainty visualisation technique. In: Proceedings of the 2nd international conference on Computer graphics and interactive techniques in Australasia and South East Asia, GRAPHITE '04, pp. 84–89. ACM Press (2004)
8. Cedilnik, A., Rheingans, P.: Procedural annotation of uncertain information. In: IEEE Visualization, pp. 77–83 (2000)
9. Chen, M.: Combining point clouds and volume objects in volume scene graphs. International Workshop on Volume Graphics pp. 127–235 (2005)
10. Cowan, C., Kovesi, P.: Automatic sensor placement from vision task requirements. Pattern Analysis and Machine Intelligence, IEEE Transactions on **10**(3), 407–416 (1988)

11. Crawfis, R., Allison, M.J.: A scientific visualization synthesizer. In: IEEE Visualization, pp. 262–267 (1991)
12. Feixas, M., Sbert, M., González, F.: A unified information-theoretic framework for viewpoint selection and mesh saliency. ACM Transactions on Application Perception **6**(1), 1:1–1:23 (2009)
13. Globus, A., Raible, E.: Fourteen ways to say nothing with scientific visualization. IEEE Computer **27**(7), 86–88 (1994)
14. Guo, H., Namee, B.M.: Using computer vision to create a 3D representation of a snooker table for televised competition broadcasting. In: Proceedings of the 18th Irish Conference on Artifical Intelligence and Cognitive Science, pp. 220–229 (2007)
15. Hartley, R.I., Zisserman, A.: Multiple View Geometry in Computer Vision, second edn. Cambridge University Press, ISBN: 0521540518 (2004)
16. Kehrer, J., Muigg, P., Doleisch, H., Hauser, H.: Interactive visual analysis of heterogeneous scientific data across an interface. IEEE Transactions on Visualization and Computer Graphics **17**(7), 934–946 (2011)
17. Kindlmann, G.: Superquadric tensor glyphs. In: Joint Eurographics - IEEE TCVG Symposium on Visualization, pp. 147–154 (2004)
18. Kirby, R.M., Marmanis, H., Laidlaw, D.H.: Visualizing multivalued data from 2D incompressible flows using concepts from painting. In: IEEE Visualization, pp. 333–340 (1999)
19. Kohlmann, P., Bruckner, S., Groller, E.M., Kanitsar, A.: Livesync: Deformed viewing spheres for knowledge-based navigation. IEEE Transactions on Visualization and Computer Graphics **13**(6), 1544–1551 (2007)
20. Legg, P.A., Parry, M.L., Chung, D.H.S., Jiang, M.R., Morris, A., Griffiths, I.W., Marshall, D., Chen, M.: From video to 3d animated reconstruction: A computer graphics application for snooker skills training. In: Eurographics (2011)
21. Legg, P.A., Parry, M.L., Chung, D.H.S., Jiang, M.R., Morris, A., Griffiths, I.W., Marshall, D., Chen, M.: Intelligent filtering by semantic importance for single-view 3d reconstruction from snooker video. In: IEEE International Conference on Image Processing, pp. 2433–2436 (2011)
22. Lodha, S.K., Pang, A., Sheehan, R.E., Wittenbrink, C.M.: UFLOW: Visualizing uncertainty in fluid flow. In: IEEE Visualization, pp. 249–254 (1996)
23. MacKinnon, D., Aitken, V., Blais, F., Picard, M.: Adaptive laser range scanning. In: Robotic and Sensors Environments, pp. 1–6 (2007)
24. McLouglin, T., Laramee, R.S., Peikert, R., Post, F.H., Chen, M.: Over two decades of integration-based geometric flow visualization. pp. 1807–1829. Blackwell Publishing Ltd (2010)
25. Morris, D.D., Kanatani, K., Kanade, T.: Gauge fixing for accurate 3D estimation. In: Computer Vision and Pattern Recognition, pp. 343–350 (2001)
26. Owens, N., Harris, C., Stennett, C.: Hawk-eye tennis system. In: International Conference on Visual Information Engineering, pp. 182–185 (2003)
27. Ozuysal, M., Lepetit, V., Fua, P.: Pose estimation for category specific multiview object localization. In: In Proceedings of Computer Vision and Pattern Recognition, pp. 778 –785 (2009)
28. Pang, A.T., Wittenbrink, C.M., Lodh, S.K.: Approaches to uncertainty visualization. The Visual Computer **13**, 370–390 (1996)
29. Parry, M.L., Legg, P.A., Chung, D.H.S., Griffiths, I.W., Chen, M.: Hierarchical event selection for video storyboards with a case study on snooker video visualization. IEEE Transactions on Visualization and Computer Graphics **17**(12), 1747–1756 (2011)
30. Putz, V., Zagar, B.: Single-Shot estimation of Camera Position and Orientation using SVD. In: Instrumentation and Measurement Technology Conference Proceedings, IEEE, pp. 1914 – 1919 (2008)
31. Rusinkiewicz, S., Hall-Holt, O., Levoy, M.: Real-time 3D model acquisition. In: SIGGRAPH 2002 Conference Proceedings, Annual Conference Series, pp. 438–446. ACM Press/ACM SIGGRAPH (2002)
32. Sanyal, J., Zhang, S., Dyer, J., Mercer, A., Amburn, P., Moorhead, R.: Noodles: A tool for visualization of numerical weather model ensemble uncertainty. IEEE Transactions on Visualization and Computer Graphics **16**(6), 1421–1430 (2010)
33. Shaw, C., Ebert, D., Kukla, J., Zwa, A., Soboroff, I., Roberts, D.: Data visualization using automatic, perceptually-motivated shapes. In: Visual Data Exploration and Analysis, SPIE (1998)
34. Taylor, R.: Visualizing multiple fields on the same surface. IEEE Computer Graphics and Applications **22**(3), 6–10 (2002)
35. Tufte, E.R.: The visual display of quantitative information. Graphics Press, Cheshire, Connecticut (1983)
36. Urness, T., Interrante, V., Longmire, E., Marusic, I., O'Neill, S., Jones, T.W.: Strategies for the visualization of multiple 2d vector fields. IEEE Computer Graphics and Applications **26**(4), 74–82 (2006)
37. Vázquez, P.P., Feixas, M., Sbert, M., Heidrich, W.: Viewpoint selection using viewpoint entropy. In: Proceedings of the Vision Modeling and Visualization Conference, pp. 273–280 (2001)
38. Verma, V., Pang, A.: Comparative flow visualization. IEEE Transactions on Visualization and Computer Graphics **10**(6), 609–624 (2004)
39. Weng, J., Ahuja, N., Huang, T.S.: Optimal motion and structure estimation. IEEE Transactions on Pattern Analysis and Machine Intelligence **15**(9), 864–84 (1993)
40. Wittenbrink, C.M., Pang, A.T., Lodha, S.K.: Glyphs for visualizing uncertainty in vector fields. IEEE Transactions on Visualization and Computer Graphics **2**(3), 266–279 (1996)
41. Zha, H., Morooka, K., Hasegawa, T., Nagata, T.: Active modeling of 3D objects: Planning on the next best pose (NBP) for acquiring range images. In: Proceedings of the International Conference on Recent Advances in 3-D Digital Imaging and Modeling, pp. 68–75 (1997)
42. Zhang, Z., Kanade, T.: Determining the epipolar geometry and its uncertainty: A review. International Journal of Computer Vision **27**, 161–195 (1998)